Structure of NKp65 bound to its keratinocyte ligand reveals basis for genetically linked recognition in natural killer gene complex

Yili Li[a,b], Qian Wang[a,b], Sharon Chen[a], Patrick H. Brown[c], and Roy A. Mariuzza[a,b,1]

[a]W. M. Keck Laboratory for Structural Biology, University of Maryland Institute for Bioscience and Biotechnology Research, Rockville, MD 20850; [b]Department of Cell Biology and Molecular Genetics, University of Maryland, College Park, MD 20742; and [c]Biomedical Engineering and Physical Sciences Shared Resource, National Institute of Biomedical Imaging and Bioengineering, National Institutes of Health, Bethesda, MD 20892

Edited* by K. Christopher Garcia, Stanford University, Stanford, CA, and approved May 22, 2013 (received for review February 27, 2013)

The natural killer (NK) gene complex (NKC) encodes numerous C-type lectin-like receptors that govern the activity of NK cells. Although some of these receptors (Ly49s, NKG2D, CD94/NKG2A) recognize MHC or MHC-like molecules, others (Nkrp1, NKRP1A, NKp80, NKp65) instead bind C-type lectin-like ligands to which they are genetically linked in the NKC. To understand the basis for this recognition, we determined the structure of human NKp65, an activating receptor implicated in the immunosurveillance of skin, bound to its NKC-encoded ligand keratinocyte-associated C-type lectin (KACL). Whereas KACL forms a homodimer resembling other C-type lectin-like dimers, NKp65 is monomeric. The binding mode in the NKp65–KACL complex, in which a monomeric receptor engages a dimeric ligand, is completely distinct from those used by Ly49s, NKG2D, or CD94/NKG2A. The structure explains the exceptionally high affinity of the NKp65–KACL interaction compared with other cell–cell interaction pairs (K_D = 6.7 × 10^{-10} M), which may compensate for the monomeric nature of NKp65 to achieve cell activation. This previously unreported structure of an NKC-encoded receptor–ligand complex, coupled with mutational analysis of the interface, establishes a docking template that is directly applicable to other genetically linked pairs in the NKC, including Nkrp1–Clr, NKRP1A–LLT1, and NKp80–AICL.

Natural killer (NK) cells are a fundamental component of innate immunity against tumors and virally infected cells. The cytolytic activity of NK cells is regulated by a dynamic interplay between activating and inhibitory signals transmitted by distinct classes of receptors that recognize both MHC and non-MHC ligands on the surface of target cells (1–3). In humans, these receptors are encoded in two distinct genomic regions: the leukocyte receptor complex (LRC) on chromosome 19 (4) and the NK gene complex (NKC) on chromosome 12 (5). The LRC codes for receptors belonging to the Ig superfamily. These include killer Ig-like receptors (KIRs), leukocyte Ig-like receptors, and the natural cytotoxicity receptor NKp46. The NKC codes for ∼30 cell-surface glycoproteins belonging to the C-type lectin-like superfamily (6). These receptors are expressed on NK and other immune-related cells, whose activity they regulate in various ways depending on cellular environment.

NKC genes have been subdivided into killer cell lectin-like receptor (KLR) genes and C-type lectin receptor (CLEC) genes (6). KLR genes encode molecules expressed on NK cells, whereas CLEC genes encode molecules expressed on other cell types (e.g., CLEC2B and CLEC9A are expressed on myeloid and dendritic cells, respectively). The KLR family includes NKG2D and CD94/NKG2A (human and rodent) and rodent Ly49s. These receptors bind classical MHC class I (MHC-I) molecules or their structural relatives and thereby facilitate detection of stressed cells or cells exhibiting aberrant MHC-I expression (5).

In addition, the KLR family includes receptors that do not engage ligands with an MHC-like fold, but instead interact with CLEC2 glycoproteins that are also members of the C-type lectin-like superfamily. These KLR and CLEC2 molecules, whose genes are intermingled in the telomeric subregion of the NKC, function as genetically linked receptor–ligand pairs. In mice, for example, the activating KLR family receptor Nkrp1f binds the CLEC2 family member Clrg, whereas the inhibitory receptor Nkrp1d binds Clrb (7, 8). Tumorigenesis and genotoxic stress down-regulate Clrb expression and thus promote NK cell-mediated lysis (8, 9). Corresponding Nkrp1–Clr receptor–ligand pairs have also been identified in humans. Thus, the inhibitory NK receptor NKRP1A (CD161), the human homolog of mouse Nkrp1d, engages the CLEC2 family member LLT1, which is expressed by activated dendritic and B cells, thereby negatively modulating NK-cell-mediated cytotoxicity (10–13). Another CLEC2 family member, AICL, is recognized by the activating NK receptor NKp80, which is genetically linked to AICL in the human NKC (14). Whereas NKp80 is found exclusively on NK cells, AICL is expressed on monocytes. The NKp80–AICL interaction promotes NK cell-mediated cytolysis of malignant myeloid cells and also mediates cellular cross-talk between NK cells and monocytes (14).

The most recent addition to the human CLEC2 family is keratinocyte-associated C-type lectin (KACL or CLEC2A), whose expression is almost exclusively restricted to the skin, in marked contrast to the broad expression of other CLEC2 family members in hematopoietic cells (15). The receptor for KACL is NKp65, a distant relative of NKp80, which is encoded adjacent to KACL in the NKC in a tail-to-tail orientation (16). Similarly to NKp80 and AICL, no related sequences for NKp65 and KACL are present in rodents, although homologs of NKp80 and KACL exist in chimpanzee, rhesus macaque, and cow (15, 17). NKp65 stimulates NK cytotoxicity and release of proinflammatory cytokines upon engagement of ectopic KACL or of KACL on freshly isolated keratinocytes. The amino terminus of the cytoplasmic domain of NKp65 contains a hemi-ITAM motif that is required for NKp65-mediated cytotoxicity (16). This Syk kinase-recruiting motif is also found in other NKC-encoded activating receptors, including dectin-1, Clec1b, and NKp80 (17–19). The genetically linked NKp65–KACL receptor–ligand pair may fulfill a dedicated role in the immune surveillance of human skin through specific recognition of keratinocytes (16, 17).

Considerable progress has been made in the structural analysis of NKC-encoded C-type lectin-like receptors that recognize MHC or MHC-related ligands (20). These structures include Ly49A bound to H-2D^d (21), Ly49C bound to H-2K^b (22, 23), NKG2D in complex with MICA (24), and NKG2A/CD94 in complex with HLA-E (25, 26). In addition, we determined the structure of killer cell lectin-like receptor G1 (KLRG1) bound to E-cadherin, a non-MHC ligand that is down-regulated in metastatic tumors (27). By contrast, no structural information is available for any of the NKC-

Author contributions: Y.L., P.H.B., and R.A.M. designed research; Y.L., Q.W., S.C., and P.H.B. performed research; Y.L., P.H.B., and R.A.M. analyzed data; and Y.L., P.H.B., and R.A.M. wrote the paper.

The authors declare no conflict of interest.

*This Direct Submission article had a prearranged editor.

Data deposition: The atomic coordinates and structure factors have been deposited in the Protein Data Bank, www.pdb.org (PDB ID code 4IOP).

[1]To whom correspondence should be addressed. E-mail: rmariuzz@umd.edu.

This article contains supporting information online at www.pnas.org/lookup/suppl/doi:10.1073/pnas.1303300110/-/DCSupplemental.

encoded receptor–ligand pairs identified to date (Nkrp1f–Clrg and Nkrp1d–Clrb in rodents and NKRP1A–LLT1, NKp80–AICL, and NKp65–KACL in humans), except for the structures of mouse Nkrp1a and Clrg in unbound form (28, 29). To understand genetically linked recognition by C-type lectin-like receptors in the NKC at the atomic level, we determined the structure of NKp65 in complex with its keratinocyte ligand KACL.

Results

Interaction of NKp65 with KACL. Human NKp65 and KACL are type II transmembrane glycoproteins, each consisting of an N-terminal intracellular domain, a transmembrane region, and an extracellular portion that comprises a 26-residue stalk and 130-residue C-type lectin-like domain (CTLD) for NKp65, and a 9-residue stalk and 117-residue CTLD for KACL. We expressed the extracellular portions of NKp65 and KACL by secretion from baculovirus-infected insect cells. Surface plasmon resonance (SPR) was used to demonstrate specific binding of NKp65 to KACL (Fig. S1*A*). Under equilibrium binding conditions, a dissociation constant (K_D) of 6.7×10^{-10} M was obtained. Kinetic parameters (on- and off-rates) for the binding of NKp65 to KACL were $k_{on} = 1.2 \times 10^6$ $M^{-1} \cdot s^{-1}$ and $k_{off} = 2.9 \times 10^{-3}$ s^{-1} (Fig. S2), giving $K_D = 2.4 \times 10^{-9}$ M, which is comparable to the K_D from equilibrium analysis. The affinity of the NKp65–KACL interaction far exceeds the affinity of other NK receptor–ligand interactions, including NKp80–AICL (2.3×10^{-6} M) (14) and NKRP1A–LLT1 (4.8×10^{-5} M) (30). Indeed, NKp65 binds KACL much more tightly than any cell–cell recognition molecules characterized to date, for which the K_D values are typically in the micromolar range (31).

To independently confirm the nanomolar affinity of the NKp65–KACL interaction from SPR, we used displacement isothermal titration calorimetry (ITC) (32). As a low-affinity reference, we engineered a double-mutant of KACL (S157A/F158A) that bound NKp65 with $K_D = 1.0 \times 10^{-6}$ M, as measured by ITC (Fig. S3*A*). Fig. S3*B* shows the integrated heats of injection for a displacement titration when wild-type KACL was injected into a calorimeter cell containing a mixture of NKp65 and KACL S157A/F158A. The best-fit K_D and 68% confidence interval from a global analysis of five datasets were 1.9×10^{-9} and 0.3–6.1×10^{-9} M, respectively, consistent with results from SPR.

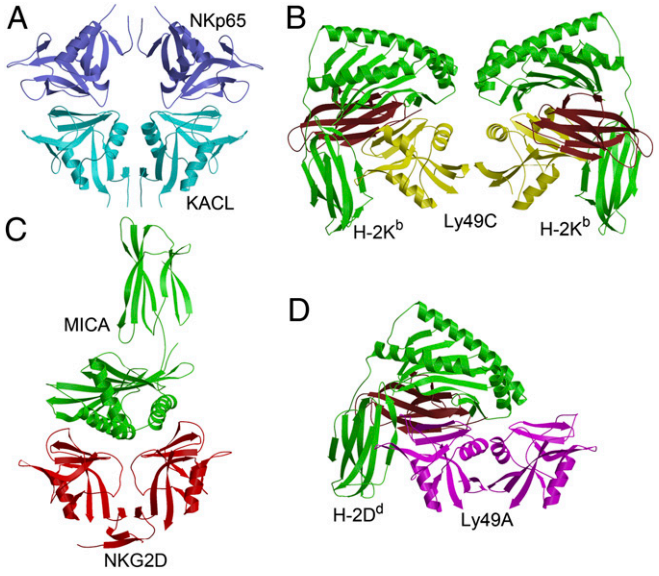

Fig. 1. Structure of the NKp65–KACL complex and comparison with other NKC-encoded receptor complexes. (*A*) Structure of the human NKp65–KACL complex. NKp65 is purple, and the KACL dimer is cyan. (*B*) Structure of the Ly49C–H-2K^b complex [Protein Data Bank (PDB) ID code 3C8K]. The Ly49C dimer is yellow, the H-2K^b heavy chain is green, and β_2-microglobulin is brown. (*C*) Structure of the NKG2D–MICA complex (PDB ID code 1HYR). The NKG2D dimer is red, and MICA is green. (*D*) Structure of the Ly49A–H-2D^d complex (PDB ID code 1QO3). The Ly49A dimer is magenta, the H-2D^d heavy chain is green, and β_2-microglobulin is brown.

Structure Determination. Recombinant NKp65 and KACL from insect cells were both heavily glycosylated and displayed considerable heterogeneity. Crystallization of the NKp65–KACL complex required extensive pretreatment of KACL with the deglycosylation enzyme peptide N-glycosidase F (PNGase F). We determined the structure of the NKp65–KACL complex to 3.2-Å resolution by molecular replacement using human lectin-like low density lipoprotein receptor-1 (LOX-1) (33) and human CD69 (34) as search models for NKp65 and KACL, respectively (Table S1 and Fig. 1*A*). Except for several residues at the N and C termini, the polypeptide chains of both NKp65 and KACL displayed continuous electron density throughout, and the NKp65–KACL interface was unambiguous (Fig. S4*A*). KACL contains three potential N-linked glycosylation sites, at residues Asn-78, -130, and -143. Clear electron density was visible for carbohydrate chains (GluNAc–GluNAc–Man) attached to Asn-78 and -130 (Fig. S4*B*). By contrast, no density corresponding to carbohydrate linked to Asn-143 was identified, most likely due to deglycosylation by PNGase. NKp65 contains two potential N-linked glycosylation sites, at Asn-67 and -202, which were not defined in the electron density map. We first describe the structures of NKp65 and KACL individually and then proceed to the NKp65–KACL complex.

Structures of NKp65 and KACL. Both NKp65 and KACL adopt a fold characteristic of other CTLDs, comprising two α-helices (α1 and α2) and two antiparallel β-sheets (Fig. 2 *A* and *B*). The two β-sheets are formed by β-strands β0, β1, and β5 and by β-strands β2, β2′, β3, and β4, respectively. There are two intrachain disulfide bonds in KACL (Cys-57–Cys-69 and Cys-86–Cys-167) and three in NKp65 (Cys-78–Cys-89, Cys-106–Cys-193 and Cys-172–Cys-185) (Fig. 3 *A* and *B*). Of these, KACL Cys-86–Cys-167 and NKp65 Cys-106–Cys-193 are invariant in all CTLDs. A Dali structure homolog search (www2.ebi.ac.uk/dali/fssp) showed that KACL is most similar to human CD69 (34, 35), an orphan C-type lectin-like protein that is also encoded in the NKC (Z score = 22; 45% sequence identity; rms difference = 1.0 Å for 117 α-carbon atoms) (Fig. 2*C*). The Z score is a measure of structural similarity based on a comparison of intramolecular distances using a sum-of-pairs method; structures with significant similarities have a Z score > 2. A comparison of KACL with mouse Clrg (29) gave similar results (Z score = 21; 47% sequence identity; rms difference = 1.1 Å for 116 α-carbon atoms). NKp65 is structurally most similar to human dendritic cell receptor CLEC9A (36) (Z score = 20; 28% sequence identity; rms difference = 1.2 Å for 116 α-carbon atoms). The structural similarity between NKp65 and mouse Nkrp1a is less pronounced (Z score = 13; 37% sequence identity; rms difference = 2.5 Å for 99 α-carbon atoms), mainly due to an extended loop in Nkrp1a (Fig. 2*D*). This loop, which corresponds to the region between strands β2 and β3 of NKp65 (Fig. 3*B*), mediates formation of a domain-swapped dimer of unknown biological function in the Nkrp1a crystal (28).

The structural similarity between NKp65 and KACL (29% sequence identity) is relatively high (rms difference = 1.6 Å for 111 α-carbon atoms) (Fig. 2 *A* and *B*). A notable difference between NKp65 and KACL resides in the L2–L3 loop that connects β-strands β2′ and β3 (Fig. 3 *A* and *B*). This loop, which corresponds to a region of high sequence and length variability among CTLDs, is two residues longer in NKp65 than in KACL and constitutes part of the interface between the two proteins in the complex. This two-residue difference in L2–L3 loop length is maintained across all known NKC-encoded receptor–ligand pairs (Fig. 3 *A* and *B*), implying a conserved overall docking topology.

The KACL Homodimer. The NKp65–KACL crystal contains one complex molecule per asymmetric unit, consisting of one NKp65 monomer and one KACL monomer. Whereas no crystallographically related dimer interface could be identified

for NKp65, two KACL monomers are related by a twofold symmetry axis to form a crystallographic dimer (Fig. S5*A*). The mode of KACL dimerization resembles that of CD69 (34), Clrg (29), and certain Ly49s (22, 23, 37): Following superposition of the KACL and CD69 dimers through one of their subunits, the orientation of the other subunits differed by only an 8° rotation (23° for KACL superposed onto Clrg; 20° for KACL superposed onto Ly49L). As in the case of CD69 and other C-type lectin family dimers, the N termini of the KACL CTLDs point in the same direction (i.e., toward the cell membrane) (Fig. S5 *A* and *B*), suggesting that the KACL crystallographic dimer represents a biologically relevant form of the ligand. By contrast, the orientation of NKp65 monomers in the NKp65–KACL complex (Fig. 1*A*) completely precludes dimerization of NKp65 in the manner of KACL or CD69.

The two subunits of KACL interact through strand β0, creating an extended antiparallel β-sheet, and through helix α2 (Fig. S5*A*). The portion of the dimer interface formed by the β0 strands includes two main-chain–main-chain hydrogen bonds linking the strands, as well as a central hydrophobic core comprising residues Leu-63, Gly-64, and Val-65 (Fig. S5*C*). In addition, Phe-104 and Tyr-108 from helix α2 pack against one another, forming a tight hydrophobic cluster at the C-terminal end of α2 (Fig. S5*D*). The total solvent-accessible surface area buried in the KACL dimer interface is 1,300 Å^2, comparable with that in CD69 (1,223 Å^2) but less than in Clrg (1,740 Å^2).

To assess the oligomeric state of KACL in solution, we used analytical ultracentrifugation (AUC) to measure the sedimentation velocity profiles for a dilution series. Fig. S6 shows an overlay of the sedimentation coefficient distributions [$c(s)$]. The distribution at lowest concentration consisted of a single peak with an average sedimentation coefficient (s_w) of 1.9 S. At the highest loading concentration, a second peak emerged near 2.5 S, and the s_w average of the entire distribution was 2.2 S. This modest concentration dependence of s_w was well described by using a monomer–dimer self-association model. Fig. S7 shows the raw sedimentation velocity data in overlay with best-fit curves for the analysis of the KACL sample at 16 μM. The fit was good, as judged by the randomness of the residuals and the magnitude of the rms deviation (0.005 OD) from the monomer–dimer model. For other KACL concentrations, rms deviations were 0.004–0.008 OD. The best-fit K_D for soluble KACL was 688 μM, with a 95% confidence interval of 287–866 μM. Although weak, this K_D may nevertheless suffice to drive dimerization of KACL in its native state, where it is anchored to the cell membrane.

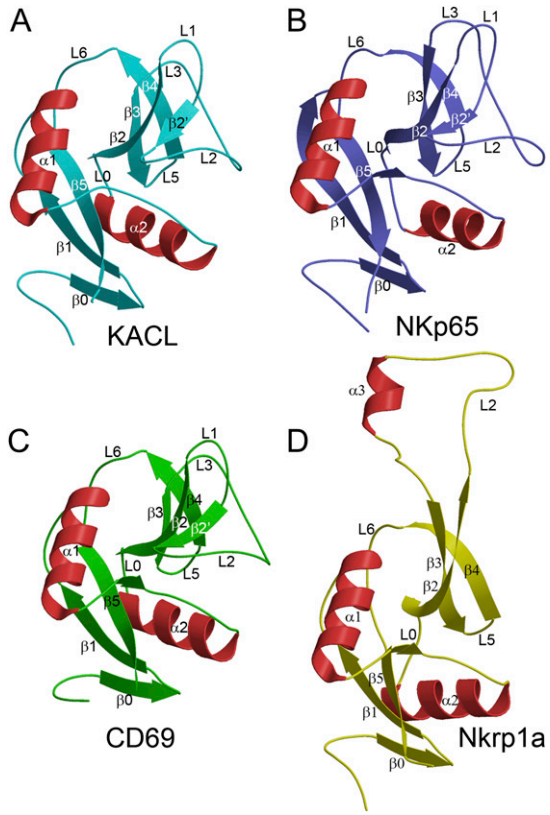

Fig. 2. Structures of KACL and NKp65. (*A*) Ribbon diagram of the KACL CTLD. Secondary structure elements are labeled. α-helices are red; β-strands and loops are cyan. (*B*) Structure of NKp65. α-helices are red; β-strands and loops are purple. (*C*) Structure of human CD69. α-helices are red; β-strands and loops are green (PDB ID code 1FM5). (*D*) Structure of mouse Nkrp1a (3M9Z). α-helices are red; β-strands and loops are yellow.

Overview of the NKp65–KACL Complex. The structure of the NKp65–KACL complex revealed that the KACL homodimer engages NKp65 bivalently, such that each KACL subunit constitutes an independent binding site for NKp65 and each NKp65 molecule makes identical contacts with KACL (Fig. 1*A*). This symmetrical, butterfly-shaped assembly is reminiscent of that of the Ly49C–H-2K^b complex (22, 23), in which the dimeric Ly49C receptor binds two MHC-I ligands symmetrically (Fig. 1*B*). However, in the NKp65–KACL complex, it is the ligand (KACL), rather than the receptor (NKp65), that constitutes the dimer.

The bivalent binding mode observed in the NKp65–KACL complex is completely distinct from those used by the dimeric NKC-encoded receptors NKG2D, CD94/NKG2A, and Ly49A. In the NKG2D–MICA complex (24), the NKG2D homodimer engages a single MICA ligand, such that the binding site of NKG2D for MICA is formed by the precise juxtaposition of two CTLD subunits (Fig. 1*C*). The binding site of CD94/NKG2A for HLA-E is constructed similarly (25, 26). In the Ly49A–H-2D^d complex (20, 21), the Ly49A homodimer engages a single H-2D^d molecule using only one its subunits (Fig. 1*D*). The structural basis for the very different modes of MHC-I engagement in the Ly49A–H-2D^d and Ly49C–H-2K^b complexes is the different dispositions of the Ly49A and Ly49C dimers. In Ly49A, as in KACL or CD69 (Fig. S5 *A* and *B*), the C-terminal ends of the α2 helices are juxtaposed, creating a closed dimer (Fig. 1*D*). In Ly49C, by contrast, the α2 helices are well separated in the dimer interface, resulting in an open conformation (Fig. 1*B*). Major steric clashes between MHC molecules would preclude the closed Ly49A dimer from simultaneously binding two MHC in the manner of the open Ly49C dimer. By contrast, the KACL dimer is able to engage two NKp65 molecules despite its closed conformation because of the much smaller size of NKp65 compared with MHC-I.

The NKp65–KACL Interface. In the NKp65–KACL complex, two structurally similar proteins use similar structural elements to bind each other in a head-to-head orientation, such that the resulting 1:1 receptor–ligand assembly resembles a symmetrical homodimer (Fig. 4*A*). The NKp65–KACL complex buries a total solvent-accessible surface area of 1,680 Å^2. The interface is characterized by relatively high shape complementarity, based on a calculated shape correlation statistic (S_c) (38) of 0.69 (S_c = 1.0 for interfaces with geometrically perfect fits), which is near the upper end of the range for protein–protein complexes and greater than the S_c values of the Ly49C–H-2K^b (0.58) (23) and NKG2A/CD94–HLA-E (0.63) interfaces (25). The mainly hydrophobic NKp65–KACL interface contains 17 hydrogen bonds (Table S2), which is considerably more than the 10 expected based on the size of the interface (39). This relative abundance of intermolecular hydrogen bonds, combined with the high shape complementarity of the interface, help explain the exceptionally high affinity of the NKp65–KACL interaction compared with other characterized interactions involving cell–cell recognition molecules.

NKp65 uses 20 residues from loops L0, L3, L5, and L6 and strands β3 and β4 to contact 16 KACL residues, also from loops L0, L3, L5, and L6 and strands β3 and β4 (Fig. 3 *A* and *B*). The

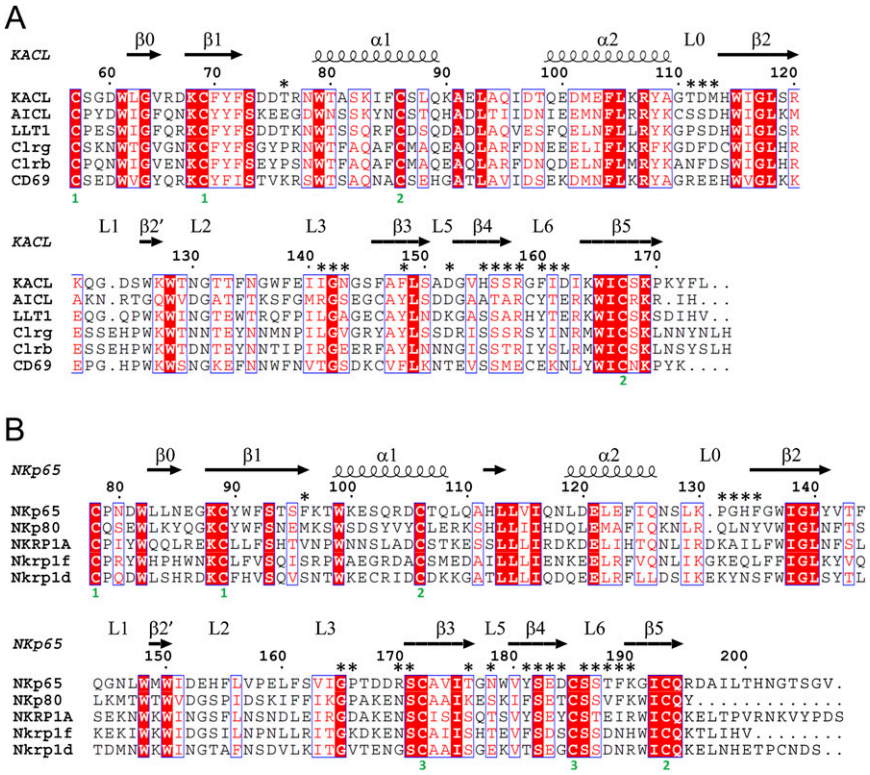

Fig. 3. Structure-based sequence alignments of NKC-encoded receptor–ligand pairs. (*A*) Sequence alignments of CTLDs of human KACL, human AICL, human LLT1, mouse Clrg, mouse Clrb, and human CD69. Secondary structure elements for KACL are denoted by squiggles (α-helices) and arrows (β-strands). These and the loop regions are numbered according to Fig. 2*A*. Residues that contact NKp65 in the NKp65–KACL complex are marked with asterisks. The paired green numbers (1 and 2) at the bottom indicate the bonded cysteine residues in the KACL structure. White characters on a red background show strictly conserved residues. Residues that are well conserved are drawn in red and framed in blue. The remaining residues are black. (*B*) Sequence alignments of CTLDs of human NKp65, human NKp80, human NKRP1A, mouse Nkrp1f, and mouse Nkrp1d. Secondary structure elements are numbered according to Fig. 2*B*. Residues that contact KACL are denoted with asterisks. The paired green numbers (1–3) indicate the bonded cysteines in the NKp65 structure. Sequences were retrieved from SwissProt via the following numbers: KACL, Q6UVW9; AICL, Q92478; LLT1, Q9UHP7, Clrg, Q9WVF9; Clrb, Q91V08; CD69, Q07108; NKp65, D3W0D1; NKp80, Q9NZS2; NKRP1A, Q12918; Nkrp1f, Q8VD98; and Nkrp1d, Q99JB4. Sequence alignments were performed with the program ClustalW (www.expasy.ch).

interface may be subdivided into three regions based on the distribution of contacting residues on KACL. In region 1, loop L0 of KACL contacts loop L0 of NKp65 (Fig. 4*B*). Residues Thr-111, Asp-112, and Met-113 of KACL loop L0, as well as Thr-76 of the loop connecting strand β1 and helix α1, make 28 total contacts with Pro-131, Gly-132 and His of NKp65 loop L0, including four hydrogen bonds (Table S2). Surprisingly, however, the side chains (at least) of KACL loop L0 residues are not energetically important for complex formation, because the triple alanine mutant T111A/D112A/M113A bound NKp65 with essentially the same affinity ($K_D = 5.3 \times 10^{-10}$ M) as wild-type KACL (6.7×10^{-10} M) (Table S3). The lack of a net contribution by these residues may be explained by their location at the periphery, rather than the center, of the protein–protein interface (40).

In region 2, Ile-141, Gly-142, and Asn-143 of KACL loop L3 make 13 contacts with Asp-184, Ser-186, Ser-187, and Thr-188 of NKp65 loop L6 (Fig. 4*C* and Table S2). These contacts are mediated primarily by main-chain atoms of KACL, including two hydrogen bonds to side-chain atoms of NKp65. In region 3, nine KACL residues from loops L5 and L6 and strands β3 and β4 contact 14 NKp65 residues, mainly from loop L6 and strand β4 (Fig. 4 *D* and *E*). Region 3 of KACL accounts for 82% (126 of 152) of the total contacts to NKp65 and 68% of the total surface buried in the interface.

To assess the functional contribution of region 3 to complex formation, eight KACL residues (Phe-148, Asp-152, His-155, Ser-157, Arg-158, Phe-160, Ile-161, and Asp-162) were mutated to alanine, individually or in combination (Table S3). Among the single alanine substitutions, the mutation D162A had the greatest effect, resulting in a 360-fold reduction in affinity ($K_D = 2.4 \times 10^{-7}$ M) (Fig. S1*B*). Asp-162 makes three hydrogen bonds through its side chain and one hydrogen bond through its main chain, as well as multiple van der Waals contacts, with NKp65 Thr-176, Asn-178, and Tyr-181 (Fig. 4*E*). Other single mutations reduced binding by 40-fold (F148A) or less (D152A, H155A). KACL Phe-148 is buried in the center of the interface with NKp65, where it makes hydrophobic contacts with NKp65 Phe-134 and -189 (Fig. 4*D*). The greatest reduction in affinity (11,000-fold) was observed for the double mutation S157A/R158A ($K_D = 7.7 \times 10^{-6}$ M) (Fig. S1*C*). This dramatic effect is probably mainly attributable to the loss of five hydrogen bonds and numerous van der Waals contacts with NKp65 mediated by the long Arg-158 side chain (Table S2). The double mutation F160A/I161A reduced binding by 550-fold ($K_D = 3.7 \times 10^{-7}$ M) (Fig. S1*D*), most likely due to the disruption of hydrophobic interactions between the side chains of the wild-type KACL residues and NKp65 Tyr-181. These mutational results validate the NKp65–KACL interface observed in the crystal structure, as well as pinpoint key binding residues (hotspots) on the ligand: Phe-148, Arg-158, Phe-160, Ile-161, and Asp-162.

Implications for Other NKC-Encoded Interaction Pairs. Besides the human NKp65–KACL interaction, several other NKC-encoded receptor–ligand pairs have now been identified: Nkrp1f–Clrg and Nkrp1d–Clrb in rodents (7, 8) and NKRP1A–LLT1 and NKp80–AICL in humans (10, 11, 14). We examined these pairs to determine whether the binding topology observed in the NKp65–KACL complex is likely to be representative of genetically linked interactions within the NKC.

The CTLD of KACL shares 49% sequence identity with that of LLT1, 42% with AICL CTLD, and 47% with Clrg CTLD (Fig. 3*A*), suggesting high structural similarity among these ligands. High structural similarity is also predicted for the CTLDs of the corresponding receptors: NKp65 is 36% identical in sequence with NKRP1A and 41% identical with NKp80 (Fig. 3*B*). Although only 2 of 16 contacting residues of KACL (Gly-142 and Arg-158) are strictly conserved in LLT1, AICL, Clrg, and Clrb, KACL Arg-158 is a hotspot residue (see above). Moreover, the corresponding residue of LLT1 (Arg-175) was shown to be critical for binding NKRP1A (30). Other hotspot residues of KACL are conservatively substituted: Phe-148 (Tyr in LLT1/AICL/Clrg/Clrb), Phe-160 (Tyr in LLT1/AICL/Clrg/Clrb), and Asp-162 (Glu in LLT1/AICL) (Fig. 3*A*). These three residues, along with KACL Arg-158, likely act as anchor points for docking different NKC-encoded receptor–ligand pairs in a conserved overall orientation, with other contacting residues of the ligands conferring specificity for particular receptors (*Discussion*).

On the receptor side of the interface, 4 of 20 contacting residues of NKp65 (Gly-165, Ser-171, -182, and -186) are strictly conserved

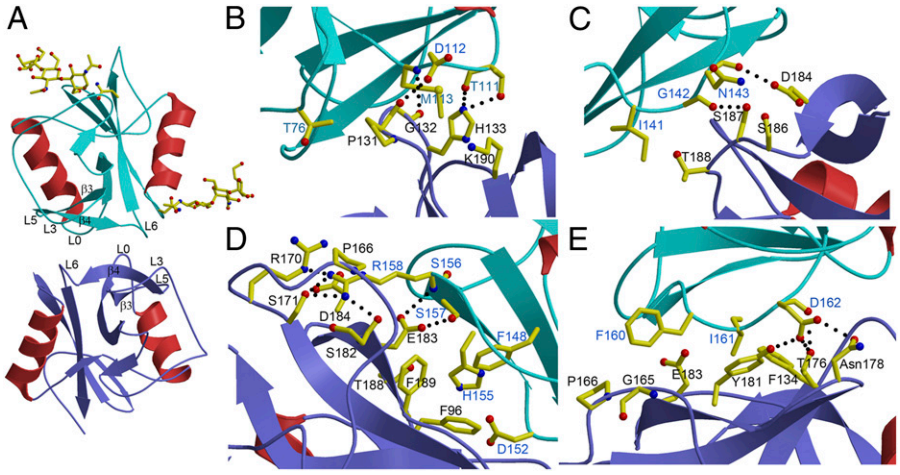

Fig. 4. The NKp65–KACL binding interface. (*A*) Structure of NKp65 bound to KACL. (*Lower*) For NKp65, β-strands and loops are purple; α-helices are red. (*Upper*) For KACL, β-strands and loops are cyan; α-helices are red. Secondary structure elements involved in contacts are labeled. Carbohydrate chains (GluNAc-GluNAc-Man) attached to Asn-78 and -130 of KACL are yellow. (*B*) Close-up view of the interactions between region 1 of KACL (cyan) and NKp65 (purple). The side chains of contacting residues are shown in ball-and-stick representation with carbon atoms in yellow, nitrogen atoms in blue, and oxygen atoms in red. Hydrogen bonds are drawn as dotted black lines. (*C*) Interactions between region 2 of KACL and NKp65. (*D*) Interactions between region 3 of KACL and NKp65, showing contacts made by loop 5 and strands β3 and β4 of KACL. (*E*) Interactions between region 3 of KACL and NKp65, showing contacts made by loop 6 of KACL.

in NKRP1A, NKp80, Nkrp1f, and Nkrp1d, whereas 3 others (Tyr-181, Glu-183, and Ser-187) are conservatively substituted (Fig. 3*B*). Most of these residues contact hotspot residues of KACL, most notably Arg-158, which forms a hydrogen-bond network with NKp65 Ser-171, -182, and Glu-183 (Table S2 and Fig. 4*D*). Furthermore, mutagenesis of NKRP1A Glu-200, which corresponds to NKp65 Glu-183, abolished binding to LLT1 (30). We conclude that the NKp65–KACL structure establishes a docking template that is generally applicable to recognition between C-type lectin-like molecules encoded in the NKC.

Discussion

In addition to carbohydrates, proteins belonging to the CTLD superfamily have been shown to selectively bind lipids, inorganic compounds, and other proteins (41). The NKp65–KACL complex is a previously unreported structural example of CTLD recognition by another CTLD, which underscores the functional versatility of this protein scaffold. In addition, the structure establishes certain constraints that must be satisfied by any mechanism proposed to describe signaling through the NKp65, NKp85, or NKPR1A pathway and the integration of these signals into the overall NK cell response.

A major difference between human NKp65 and mouse Nkrp1a is that Nkrp1a crystallized as a domain-swapped dimer in which domain swapping was mediated by an extended loop pointing away from the CTLD that corresponds to the region between strands β2 and β3 of NKp65 (28), which includes several key KACL-contacting residues. The domain-swapped Nkrp1a dimer is sterically incompatible with ligand binding in the manner of NKp65 and may be a crystallization artifact, as sometimes observed for fragments of complete proteins (such as the Nkrp1a CTLD) under the high concentrations (42). Indeed, solution-based biophysical data did not support the oligomeric state of Nkrp1a observed in the crystal (28).

In the mouse, Nkrp1f recognizes Clrg, whereas Nkrp1d recognizes Clrb (7, 8). The source of these specificity differences may be examined in terms of the NKp65–KACL complex. Clrg differs from Clrb at 7 of 16 predicted Nkrp1f-contacting residues, of which 3 are conservatively substituted (Clrg111D/Clrb111N, Clrg152D/Clrb152N, and Clrg157S/Clrb157T) (Fig. 3*A*). Of the nonconservative substitutions, Clrg141L/Clrb141R is predicted to contact a single residue (Asp-188) that is identical in Nkrp1f and Nkrp1d (Fig. 3*B* and Table S2). Likewise, based on the NKp65–KACL structure, Clrg142V/Clrb142E should contact two identical residues (Ser-186 and -187) of Nkrp1f and Nkrp1d. By contrast, Clrg161I/Clrb161S and Clrg162N/Clrb162L, which correspond to hotspot residues in loop 6 of KACL, are expected to interact with a tight cluster of nonconservatively substituted residues in strands β2 (Nrp1f134L/Nkrp1d134S) and β4 (Nkrp1f181F/Nkrp1d181T) and loop L5 (Nkrp1f178T/Nkrp1d178E) of the receptor (Fig. 4*E*). We propose that Nkrp1 receptors discriminate between Clr ligands by focusing recognition on sequence differences at Clr positions 161 and 162.

Mutational analysis of KACL identified five hotspot residues on the ligand: Phe-148, Arg-158, Phe-160, Ile-161, and Asp-162. These residues are strictly conserved (Arg-158) or conservatively substituted among KACL, AICL, and LLT1, respectively: F/Y/Y148, F/Y/Y160, I/T/T161, and D/E/E162 (Fig. 3*A*). Moreover, these hotspot residues contact residues on the NKp65, NKp80, and NKRP1A receptors that are themselves strictly or highly conserved. Consequently, these residues likely maintain a conserved docking orientation in the NKp65–KACL, NKp80–AICL, and NKRP1A–LLT1 complexes, whereas other less conserved residues confer specificity. Among the 20 NKp65 residues that contact KACL, 5 are especially variable among NKp65, NKp80, and NKRP1A, respectively: P/Q/K131, G/L/A132, H/N/I133, and D/T/Y184, and T/V/E188 (Fig. 3*B*). The corresponding contacting residues on KACL, AICL, and LLT1 display similar variability. We conclude that NKp65, NKp80, and NKRP1A discriminate among their NKC-encoded ligands through sequence differences at receptor positions 131–133, 184, and/or 188.

The affinity of NKp65 for KACL ($K_D = 6.7 \times 10^{-10}$ M) is 3,000-fold greater than that of NKp80 for AICL (14) and 70,000-fold greater than that of NKRP1A for LLT1 (30). It also far exceeds the affinity of any other known NK cell receptor–ligand pair, including NKG2D–MICA, Ly49–MHC-I, KIR–MHC-I, CD94/NKG2–HLA-E, and 2B4–CD48 (23, 25, 43–45). NKp80 and NKRP1A, as well as other C-type lectin-like NK receptors (NKG2D, Ly49, CD94/NKG2), all exist as disulfide-linked dimers on the cell surface. These interchain disulfide bonds are formed between paired cysteines within the stem regions of the receptors. In marked contrast, NKp65 is not disulfide-linked on NK cells (16), and the NKp65 CTLD is monomeric both in the NKp65–KACL structure and in solution. Similarly, AICL and LLT1 (10, 11, 14), but not KACL (16), exist as disulfide-linked dimers on target cells, although the KACL CTLD did crystallize as a noncovalent dimer and formed non-disulfide-linked dimers in solution.

We propose that these differences in dimerization state reflect fundamentally different strategies for achieving NK-cell activation. Thus, dimerization of NKp80 and NKRP1A on the cell surface may increase their avidity for AICL and LLT1 through bivalent binding, thereby compensating for the low intrinsic affinities of these receptors relative to NKp65. By contrast, the high monomeric affinity of NKp65 for KACL may overcome the need for receptor dimerization by generating complexes with half-life and signaling capacity similar to those of the NKp80–AICL and NKRP1A–LLT1 complexes. Thus, signaling through NKp65, NKp85, or NKPR1A may proceed via different mechanisms, even though these receptors engage their respective ligands using a conserved docking topology.

Materials and Methods

Protein Production and Purification. Soluble NKp65 and KACL were expressed by secretion from baculovirus-infected insect cells (*SI Materials and Methods*).

Crystallization and Structure Determination. The NKp65–KACL complex was crystallized following deglycosylation of KACL. The structure of the complex was determined by molecular replacement (*SI Materials and Methods*).

SPR Analysis. The affinity of NKp65 for wild-type KACL or KACL mutants was measured by SPR with a BIAcore T100 biosensor (*SI Materials and Methods*).

ITC Analysis. Displacement ITC (32) was used to measure the high-affinity binding interaction between NKp65 and wild-type KACL (*SI Materials and Methods*).

AUC Analysis. The oligomeric state of KACL in solution was assessed by sedimentation velocity AUC (*SI Materials and Methods*).

ACKNOWLEDGMENTS. We thank H. Robinson (Brookhaven National Synchrotron Light Source) for X-ray data collection. Support for beamline X29 comes from the Offices of Biological and Environmental Research and of Basic Energy Sciences of the Department of Energy, and from the National Center for Research Resources of the National Institutes of Health. This study was supported by National Institutes of Health Grant AI047990 (to R.A.M.).

1. Lanier LL (2008) Up on the tightrope: Natural killer cell activation and inhibition. *Nat Immunol* 9(5):495–502.
2. Bryceson YT, Long EO (2008) Line of attack: NK cell specificity and integration of signals. *Curr Opin Immunol* 20(3):344–352.
3. Vivier E, Ugolini S, Blaise D, Chabannon C, Brossay L (2012) Targeting natural killer cells and natural killer T cells in cancer. *Nat Rev Immunol* 12(4):239–252.
4. Kelley J, Walter L, Trowsdale J (2005) Comparative genomics of natural killer cell receptor gene clusters. *PLoS Genet* 1(2):129–139.
5. Yokoyama WM, Plougastel BFM (2003) Immune functions encoded by the natural killer gene complex. *Nat Rev Immunol* 3(4):304–316.
6. Hao L, Klein J, Nei M (2006) Heterogeneous but conserved natural killer receptor gene complexes in four major orders of mammals. *Proc Natl Acad Sci USA* 103(9):3192–3197.
7. Iizuka K, Naidenko OV, Plougastel BF, Fremont DH, Yokoyama WM (2003) Genetically linked C-type lectin-related ligands for the NKRP1 family of natural killer cell receptors. *Nat Immunol* 4(8):801–807.
8. Carlyle JR, et al. (2004) Missing self-recognition of Ocil/Clr-b by inhibitory NKR-P1 natural killer cell receptors. *Proc Natl Acad Sci USA* 101(10):3527–3532.
9. Fine JH, et al. (2010) Chemotherapy-induced genotoxic stress promotes sensitivity to natural killer cell cytotoxicity by enabling missing-self recognition. *Cancer Res* 70(18): 7102–7113.
10. Aldemir H, et al. (2005) Cutting edge: Lectin-like transcript 1 is a ligand for the CD161 receptor. *J Immunol* 175(12):7791–7795.
11. Rosen DB, et al. (2005) Cutting edge: Lectin-like transcript-1 is a ligand for the inhibitory human NKR-P1A receptor. *J Immunol* 175(12):7796–7799.
12. Rosen DB, et al. (2008) Functional consequences of interactions between human NKR-P1A and its ligand LLT1 expressed on activated dendritic cells and B cells. *J Immunol* 180(10):6508–6517.
13. Germain C, et al. (2011) Induction of lectin-like transcript 1 (LLT1) protein cell surface expression by pathogens and interferon-γ contributes to modulate immune responses. *J Biol Chem* 286(44):37964–37975.
14. Welte S, Kuttruff S, Waldhauer I, Steinle A (2006) Mutual activation of natural killer cells and monocytes mediated by NKp80-AICL interaction. *Nat Immunol* 7(12):1334–1342.
15. Spreu J, Kienle EC, Schrage B, Steinle A (2007) CLEC2A: A novel, alternatively spliced and skin-associated member of the NKC-encoded AICL-CD69-LLT1 family. *Immunogenetics* 59(12):903–912.
16. Spreu J, et al. (2010) Interaction of C-type lectin-like receptors NKp65 and KACL facilitates dedicated immune recognition of human keratinocytes. *Proc Natl Acad Sci USA* 107(11):5100–5105.
17. Vogler I, Steinle A (2011) Vis-à-vis in the NKC: Genetically linked natural killer cell receptor/ligand pairs in the natural killer gene complex (NKC). *J Innate Immun* 3(3): 227–235.
18. Fuller GL, et al. (2007) The C-type lectin receptors CLEC-2 and Dectin-1, but not DC-SIGN, signal via a novel YXXL-dependent signaling cascade. *J Biol Chem* 282(17): 12397–12409.
19. Dennehy KM, Klimosch SN, Steinle A (2011) Cutting edge: NKp80 uses an atypical hemi-ITAM to trigger NK cytotoxicity. *J Immunol* 186(2):657–661.
20. Deng L, Mariuzza RA (2006) Structural basis for recognition of MHC and MHC-like ligands by natural killer cell receptors. *Semin Immunol* 18(3):159–166.
21. Tormo J, Natarajan K, Margulies DH, Mariuzza RA (1999) Crystal structure of a lectin-like natural killer cell receptor bound to its MHC class I ligand. *Nature* 402(6762):623–631.
22. Dam J, et al. (2003) Variable MHC class I engagement by Ly49 NK receptors revealed by the crystal structure of Ly49C bound to H-2K^b. *Nat Immunol* 12:1213–1222.
23. Deng L, et al. (2008) Molecular architecture of the MHC-binding site of Ly49 natural killer cell receptors. *J Biol Chem* 283:16840–16849.
24. Li P, et al. (2001) Complex structure of the activating immunoreceptor NKG2D and its MHC class I-like ligand MICA. *Nat Immunol* 2(5):443–451.
25. Petrie EJ, et al. (2008) CD94-NKG2A recognition of human leukocyte antigen (HLA)-E bound to an HLA class I leader sequence. *J Exp Med* 205(3):725–735.
26. Kaiser BK, Pizarro JC, Kerns J, Strong RK (2008) Structural basis for NKG2A/CD94 recognition of HLA-E. *Proc Natl Acad Sci USA* 105(18):6696–6701.
27. Li Y, et al. (2009) Structure of natural killer cell receptor KLRG1 bound to E-cadherin reveals basis for MHC-independent missing self recognition. *Immunity* 31(1):35–46.
28. Kolenko P, et al. (2011) Molecular architecture of mouse activating NKR-P1 receptors. *J Struct Biol* 175(3):434–441.
29. Skálová T, et al. (2012) Mouse Clr-g, a ligand for NK cell activation receptor NKR-P1F: crystal structure and biophysical properties. *J Immunol* 189(10):4881–4889.
30. Kamishikiryo J, Fukuhara H, Okabe Y, Kuroki K, Maenaka K (2011) Molecular basis for LLT1 protein recognition by human CD161 protein (NKRP1A/KLRB1). *J Biol Chem* 286(27):23823–23830.
31. Davis SJ, et al. (2003) The nature of molecular recognition by T cells. *Nat Immunol* 4(3):217–224.
32. Sigurskjold BW (2000) Exact analysis of competition ligand binding by displacement isothermal titration calorimetry. *Anal Biochem* 277(2):260–266.
33. Park H, Adsit FG, Boyington JC (2005) The 1.4 angstrom crystal structure of the human oxidized low density lipoprotein receptor lox-1. *J Biol Chem* 280(14):13593–13599.
34. Natarajan K, Sawicki MW, Margulies DH, Mariuzza RA (2000) Crystal structure of human CD69: A C-type lectin-like activation marker of hematopoietic cells. *Biochemistry* 39(48):14779–14786.
35. Llera AS, Viedma F, Sánchez-Madrid F, Tormo J (2001) Crystal structure of the C-type lectin-like domain from the human hematopoietic cell receptor CD69. *J Biol Chem* 276(10):7312–7319.
36. Zhang JG, et al. (2012) The dendritic cell receptor Clec9A binds damaged cells via exposed actin filaments. *Immunity* 36(4):646–657.
37. Back J, et al. (2009) Distinct conformations of Ly49 natural killer cell receptors mediate MHC class I recognition in *trans* and *cis*. *Immunity* 31(4):598–608.
38. Lawrence MC, Colman PM (1993) Shape complementarity at protein/protein interfaces. *J Mol Biol* 234(4):946–950.
39. Wodak SJ, Janin J (2002) Structural basis of macromolecular recognition. *Adv Protein Chem* 61:9–73.
40. Dall'Acqua W, et al. (1998) A mutational analysis of binding interactions in an antigen-antibody protein-protein complex. *Biochemistry* 37(22):7981–7991.
41. Zelensky AN, Gready JE (2005) The C-type lectin-like domain superfamily. *FEBS J* 272(24):6179–6217.
42. Huang Y, Cao H, Liu Z (2012) Three-dimensional domain swapping in the protein structure space. *Proteins* 80(6):1610–1619.
43. Lengyel CS, et al. (2007) Mutations designed to destabilize the receptor-bound conformation increase MICA-NKG2D association rate and affinity. *J Biol Chem* 282(42): 30658–30666.
44. Boyington JC, Motyka SA, Schuck P, Brooks AG, Sun PD (2000) Crystal structure of an NK cell immunoglobulin-like receptor in complex with its class I MHC ligand. *Nature* 405(6786):537–543.
45. Velikovsky CA, et al. (2007) Structure of natural killer receptor 2B4 bound to CD48 reveals basis for heterophilic recognition in signaling lymphocyte activation molecule family. *Immunity* 27(4):572–584.